DOI: 10.1002/ ((please add manuscript number))
Article type: Research Article

Robust and Multifunctional Kirigami Electronics with Tough and Permeable Aramid Nanofiber Framework

*Hongzhen Liu,[#] Hegeng Li,[#] Zuochen Wang,[#] Xi Wei, Hengjia Zhu, Mingze Sun, Yuan Lin, and Lizhi Xu**

H. Liu, H. Li, Dr. Z. Wang, Dr. X. Wei, H. Zhu, M. Sun, Prof. Y. Lin, Prof. L. Xu
Department of Mechanical Engineering
The University of Hong Kong
Hong Kong SAR 999077, China
E-mail: L. Xu, xulizhi@hku.hk

Dr. Z. Wang, Dr. X. Wei, Prof. Y. Lin, Prof. L. Xu
Advanced Biomedical Instrumentation Centre Limited
Hong Kong SAR 999077, China.

These authors contributed equally: Hongzhen Liu, Hegeng Li and Zuochen Wang.

Keywords: stretchable electronics, kirigami electronics, fracture resistance, nanofiber framework, wearable systems

Abstract:

Kirigami designs are advantageous for the construction of wearable electronics due to their high stretchability and conformability on 3D dynamic surfaces of the skin. However, suitable materials technologies that enable robust kirigami devices with desired functionality for skin-interfaces remain limited. Here, a versatile materials platform based on composite nanofiber framework (CNFF) was exploited for the engineering of wearable kirigami electronics. The self-assembled fibrillar network involving aramid nanofibers and polyvinyl alcohol combines high toughness, permeability, and manufacturability, which are desirable for the fabrication of hybrid devices. Multiscale simulations were conducted to explain the high fracture resistance of CNFF-based kirigami structures and provided essential guidance for the design, which can be further generalized to other kirigami devices. Various microelectronic sensors and electroactive polymers were integrated onto CNFF-based materials platform to achieve measurements of electrocardiogram (ECG), electromyogram (EMG), skin

temperature, and other physiological parameters. These mechanically robust, multifunctional, lightweight, and biocompatible kirigami devices could shed new insights for the development of advanced wearable systems and human-machine interfaces.

1. Introduction

Stretchable electronics are useful for the construction of smart wearable systems due to their mechanical compatibility with dynamic surfaces of the human body.[1–4] Although a variety of materials and structural designs were exploited for the fabrication of stretchable electronics, achieving high mechanical robustness with desired functionality for wearable applications remains challenging. For instance, conjugated polymers and soft composites exhibit considerable electrical conductance even under severe deformation,[5–7] but fabrication of multifunctional polymer devices with stress-invariant electronic properties is difficult. Filamentary serpentine meshes with inorganic components combines excellent electronic performance and good stretchability,[8,9] but their delicate structures are prone to mechanical damage. Transfer printing of serpentine electronics onto elastomer films could enhance their overall structural robustness.[10,11] However, the dense polymer substrate may hinder water and vapor transport arising from biological tissues, causing potential issues for wearable applications.[12–15] In addition, poor conformability of dense films on non-developable 3D surfaces is another limitation.[16,17]

Kirigami-inspired structures have recently emerged as promising candidates for stretchable electronics.[18–23] In kirigami devices, a pattern of cuts is introduced into solid membranes, which allows the whole structure to accommodate imposed macroscopic elongation via mesoscale bending and twisting. Furthermore, kirigami membranes are capable of large-area integration on 3D dynamic surfaces,[24,25] providing a conformal platform for wearable human-machine interfaces.

However, designing robust and multifunctional kirigami electronics for wearable applications imposes strict restrictions on the constituent materials. Firstly, the cuts involved in kirigami patterning inevitably lead to stress concentration in the materials under stretching, potentially causing failure of the device by crack propagation. Therefore, many electronic materials with brittle nature may not be suitable for creating kirigami membranes with high stretchability. A careful evaluation regarding the stretchable design and intrinsic toughness of the base materials becomes essential. Secondly, fabrication methods must be developed for reliable integration of diverse functional electronic components onto the base membrane. In this regard, an ideal material platform should be compatible with both the transferred inorganic microelectronics and conductive composites involving soft polymers, along with their distinct processing techniques. Thirdly, microstructural permeability of the membrane is desired, which combines with the mesoscale openings from kirigami cuts to provide breathability of the device for wearable applications.

Herein, we report a versatile materials platform for the construction of wearable kirigami electronics with high mechanical robustness and multifunctionality (**Figure 1a**). A central piece in this platform is a microporous framework based on aramid nanofiber (ANF) composites.[26,27] The self-assembled hyperconnective fibrillar network exhibits high toughness to withstand stress concentration around kirigami cuts, allowing flexible design for stretchability without causing failure of the device by crack propagation. The solution-based processing steps for fabricating microporous kirigami membranes make their integration with various integrated electronic components, including transfer-printed inorganic microelectronics and infiltrated conducting polymers, very feasible (**Figure 1b and c**). The multifunctional kirigami electronics are compatible with 3D surfaces of the skin, enabling physiological sensing of electrocardiogram (ECG), electromyogram (EMG), skin temperature, and potentially other important parameters. These robust, multifunctional, and biocompatible

kirigami devices may provide insights for the design of advanced stretchable electronics and wearable systems.

2. Results and Discussion

Mechanical behaviors of the base materials are critically important for the engineering of kirigami membranes. The composite nanofiber framework (CNFF) exhibits unique properties originating from the interactions between its nanoscale constituents, i.e., hydrogen bonding between stiff ANFs and flexible polyvinyl alcohol (PVA) (**Figure S1**). Solution-based processing followed by critical point drying (CPD) enables self-assembly of hyperconnective 3D network with strong welded fibrillar joints and high nodal connectivity.[27] These microstructural features are crucial for the macroscopic strength and toughness of porous composites.[28,29] Indeed, CNFF membranes (~100 μm in thickness) without kirigami cuts exhibit high ductility (~107 %) and strength (~7.16 MPa) under tension (**Figure 2a**). Their fracture energy (~1500 J/m^2) can be an order of magnitude higher than those of common polymers in electronics (e.g., SU-8), and it is comparable to that of natural rubber (**Figure 2b**).[30,31] The mechanical behaviours of CNFF can be further modified by tuning the concentrations of ANFs and PVA in the liquid precursor. A stretchable kirigami membrane from CNFF can bear loads ~1,000 times higher than its own weight without mechanical failure or propagation of the cuts (**Figure 2c**).

Microstructural examination of the fracture processes revealed the origin of the high toughness of CNFF. Interestingly, fracture of CNFF follows a tortuous path (**Figure 2d**), indicating its high capability of strain energy dissipation. In addition, blunting of the crack tip and alignment of fibrils at the crack front were observed (**Figure 2e and f**), which help to reduce stress concentration and resist further propagation of the crack. These observations are consistent with the network topology and nodal mechanics of CNFF. Specifically, the random

nature of the 3D hyperconnective network is helpful for the deflection of crack propagation. On the other hand, the high nodal strength affords reorientation of fibrils without early breakage of their joints, which effectively transfers mechanical loads and mitigates the stress field induced around the crack tip.

We developed computational models to further examine the effects of fibrillar interactions on the toughness of CNFF. Specifically, a random network was generated with linear and rotational springs crosslinking each pair of intersecting fibrils.[32,33] Binding energy was defined as the critical elastic energy stored in the springs before breakage of the crosslinks, reflecting strength of the fibrillar joint. We introduced an initial crack and simulated the responses of the fibrillar network under imposed elongation (**Figure 2g**). With initial geometry of the network and stiffness of crosslinkers kept constant, high binding energy led to blunting and alignment of fibrils near the crack tip under imposed stretching (**Figure 2h**), which is consistent with the experimental observations. In contrast, reducing the binding energy by 60% resulted in an early rupture of the network and much less re-orientation of the fibrils (**Figure S2**).

The high toughness of CNFF is crucial for the structural robustness of kirigami membranes under deformation. Using finite element analysis (FEA), we evaluated energy release rates for the extension of cuts and compared them with the intrinsic fracture energy of the base material (e.g., CNFF), which provides a quantitative indicator of fracture resistance. Not surprisingly, under stretching, the sharp cuts introduced in the membrane create a driving force for crack propagation, with an energy release rate increasing with the imposed elongation (**Figure 2i and Figure S3**). Nevertheless, the fracture energy of CNFF (~1500 J/m^2) is about two times higher than the energy release rate for crack propagation even when the imposed elongation reaches 90%, and therefore prevents propagation of the cuts. In addition, the strain distributed in the membrane is well below the failure strain of CNFF, indicating high stretchability of the structure (**Figure 2j**). In contrast, kirigami membranes

based on other electronic materials, such as single-crystal silicon or SU-8 epoxy, cannot achieve such level of structural robustness. Specifically, with the same set of geometrical designs, the simulated energy release rates exceeded the intrinsic fracture energy of the constituent materials (e.g., ~10 J/m^2 for silicon or ~107 J/m^2 for SU-8) even at low levels of stretching (<10%) (**Figure S4**), suggesting early onset of crack propagation and potential failure of the device.[31,34,35] Indeed, the driving force for fracture in kirigami structures is dependent on various parameters including the geometrical configuration of the cuts, the degree of imposed elongation, as well as the stiffness of the constituent materials, etc. Therefore, careful evaluation of specific designs with reference to the intrinsic fracture toughness of the constituent materials is important.

The outstanding mechanical properties and processability of CNFF allow reliable fabrication of multifunctional kirigami electronics. Indeed, liquid mixture of ANFs and PVA in dimethyl sulfoxide (DMSO) can be blade-coated or spin-coated, forming uniform membrane substrates. The hydroxyl groups on PVA are available for chemical interactions with other surfaces, allowing for strong bonding with to transferred electronic devices, with an interfacial toughness of ~20 J/m^2 (**Figure S5**). Furthermore, the porous CNFF affords infiltration of other functional materials to generate mechanically robust and electroactive composites for devices applications. In the present study, we developed diverse routes for the fabrication of CNFF-based kirigami electronics (**Figure 3**). Specifically, multifunctional devices involving inorganic electronic materials were microfabricated on a planar wafer coated with a sacrificial layer (e.g., polymethylmethacrylate, PMMA) (**Figure 3a and Figure S6-S8**). The electronics were encapsulated with polyimide (PI) layers to prevent current leakage and to allow subsequent chemical functionalization of the surfaces. After dissolving the sacrificial layer, the electronic components were picked up from the handling wafer with a soft stamp (e.g., water-soluble tape). Treatment of oxygen plasma on the stamp-supported devices generates hydroxyl groups on the surfaces for further chemical interactions with the

polymers in CNFF. Blade-coating a layer of liquid precursor of CNFF followed by solvent exchange with water yielded a hydrogel membrane firmly bonded with the electronic components.

In another fabrication scheme, conducting polymers can be selectively deposited into the porous network of CNFF through electrochemical methods (**Figure 3b and Figure S9**). Specifically, a conductive substrate (e.g., steel plate) was masked with a laser-scribed insulating tape, with the openings defining the patterns for conductive surface. Blade-coating a layer of liquid precursor of CNFF followed by solvent exchange led to a hydrogel membrane attached to the masked substrate. Next, the sample was immersed into an aqueous solution of monomers of interest (e.g., 3,4-ethylenedioxythiophene, EDOT). Applying appropriate potential and current (**Figure S10**) through the conductive substrate led to conducting polymers (e.g., poly(3,4-ethylenedioxythiophene), PEDOT) deposited into the porous network of ANF-PVA, with the patterns defined by the mask. The interpenetrating microstructures involving nanofiber networks and conducting polymers afford strong interfacial bonding and high structural robustness under mechanical loads (**Figure S10 and S11**). These conductive patterns can serve as electrodes or interconnects for further applications.

To complete the fabrication of CNFF-based kirigami electronics, the device-bonded hydrogel membranes were laser-cut halfway through their thickness with kirigami patterns. This method preserves the geometry of the membrane during the shrinking process involved in CPD. After the drying process, the laser-scribed area of CNFF was fully removed, leading to highly stretchable kirigami electronics.

We evaluated the performance of CNFF-based kirigami electronics in the context of wearable applications. The stretchability of kirigami membranes scales with $(L_c\text{-}x)/2y$, where L_c is the length of the cut, x is the spacing between nearest cuts in the transverse direction, and y is the spacing in the axial direction.[19] Modifying the kirigami patterns allows for tuning of

the stretchability of the membranes (**Figure S12**). To further reduce stress concentration under stretching, round edges of the kirigami cuts were designed for the fabricated devices (**Figure S13-15**). We evaluated the fracture resistance of the design by introducing cracks at the tip of the round edges in the FEA modeling of stretching. The simulated energy release rate remains an order of magnitude lower than the fracture energy of CNFF even under 100% of elongation, indicating sufficient structural robustness (**Figure S16**). During experimental tensile tests, the behaviors of the kirigami membrane were barely influenced by the printed electronic components, but instead were largely determined by the intrinsic properties of CNFF as well as the structural design of the kirigami patterning (**Figure 4a**). At low strains (<5%), the initial stiffness (~ 94.6 kPa) of the membrane is due to the stretching of CNFF. As the load reaches a threshold for triggering buckling, the deformation is mostly dominated by the out-of-plane deformation of the kirigami structures, leading to a low effective stiffness of ~19.7 kPa. Finally, the membrane failed at very high elongation due to tearing at the edge of kirigami cuts.

CNFF-based kirigami electronics exhibit stretching-invariant electrical properties. The resistance of serpentine interconnects in a kirigami membrane remains unchanged even under 130% of elongation (**Figure 4b**). Indeed, the structural deformation of both the kirigami membrane and the serpentine interconnects accommodated the macroscopic elongation and led to low strains in the constituent materials. In contrast, serpentine interconnects bonded to a continuous membrane without kirigami patterning failed at a lower elongation of ~60%. Furthermore, CNFF-based kirigami electronics can withstand over 5,000 cycles of 60% elongation without causing significant change to the electrical resistance (**Figure 4c**).

The high deformability of CNFF-based kirigami electronics enables conformal integration of the devices on the dynamic 3D surfaces of the skin (**Figure 4d and e**). Additional gel adhesives can be applied to further strengthen the interface between the devices and the skin. The kirigami patterns accommodated 3D deformation and led to

minimal driving force for interfacial delamination. The porous microstructures of CNFF allow vapor transport, which was confirmed by characterization of air flow through CNFF membranes. Specifically, under a face velocity of 0.05m/s, the presence of CNFF membrane led to a moderate pressure drop ranging from 2 kPa to 10 kPa, corresponding to a thickness of membrane ranging from 20 μm to 200 μm (**Figure 4f**). It is conceivable that the intrinsic permeability of CNFF membranes, in conjunction with the structural openings created by kirigami cuts, enhances their breathability during extended wearing on the skin. The low density of CNFF (~0.15 g/cm^3) is also beneficial for wearable applications. In addition, the viability of NIH 3T3 fibroblasts cultured on CNFF indicates good biocompatibility of CNFF-based kirigami devices (**Figure 4g and h**).

The multifunctional electronics built in CNFF-based kirigami devices enable characterization of various physiological information from the skin (**Figure 5a and Figure S17-18**). For example, the contact impedance between electrodes and the skin ranges from 120 kΩ to 180 kΩ at 100 Hz, which is sufficient for gathering high-quality electrophysiological signals (**Figure S19a**). Indeed, electrocardiogram (ECG) signals captured by both transfer-printed gold (Au) electrodes and infiltrated PEDOT electrodes exhibited clean details comparable to those measured with commercial silver/silver chloride (Ag/AgCl) gel electrodes (**Figure 5b**). An array of microfabricated electrodes laminated on the forearm can be used for the recording of electromyogram (EMG) (**Figure 5c**). EMG signals measured from different pairs of electrodes captured the distinct patterns arising from contraction of different muscle groups (**Figure 5d and e**). This spatiotemporal information can be useful for gesture recognition or other applications for human-machine interactions. Thermal sensors in the array are based on the temperature coefficient of resistance for gold traces (**Figure S19 b**). They were able to capture temperature variations in physiologically relevant processes, represented by a hot compress applied to the skin (**Figure 5f**).

3. Conclusion

In summary, we have developed a versatile CNFF-based material platform for the construction of kirigami electronics for wearable applications. The high toughness, permeability, and processability of CNFF are advantageous for the development of robust and multifunctional kirigami membranes that conform well to 3D dynamic surfaces of the skin. The mechanics insights regarding the fracture resistance of CNFF-based devices revealed here are also applicable to the engineering of other kirigami devices, and therefore provide guidance for their design and fabrication. Due to the manufacturability of CNFF-based devices, their capability of physiological sensing and stimulation can be further expanded. Inclusion of high-density electrodes array, actuators, microfluidics, or biochemical sensors is highly feasible, which could enable sophisticated wearable system for medical diagnosis, disease management, human-machine interactions, or other advanced applications.

4. Methods

Fabrication of CNFF-based kirigami electronics

2 wt% ANF dispersed in DMSO and 10 wt% PVA solution in DMSO were prepared using established methods.[27,36] These two liquids were mixed in a water-free environment with 1:1 volume ratio to obtain liquid ANF-PVA mixture. The liquid precursor was then blade-coated with controlled thickness followed by immersing in deionized water to generate ANF-PVA hydrogel membranes. Kirigami pattern was introduced into the hydrogel membrane by laser cutting. After that, hydrogel membranes with kirigami pattern were immersed in ethanol for 12 h followed by CPD to generate CNFF membranes. The laser-scribed area was mechanically removed to complete the kirigami structures. Scanning electron microscopy (SEM, Hitachi S4800) was used to characterize the 3D microstructures on CNFF.

Various methods, including thin-film deposition, photolithography and etching, have been developed for the microfabrication of electronics.[37] In the present study, water-soluble tapes (3M) were used as stamps to pick up microfabricated electronics from the handling wafer. Next, the stamp-supported electronics were treated with oxygen plasma (Tailong Electronics, China) and then blade-coated with a layer of liquid mixture of ANF-PVA. Finally, the tape-supported electronics covered with the mixture were immersed in deionized water to release the tape and solidify the ANF-PVA, leading to hydrogel-bonded electronics.

PET tapes was patterned with laser cutting and attached to a steel plate, serving as the mask for electrodeposition of PEDOT. ANF-PVA hydrogel attached on the mask was fabricated by blade coating and solvent exchange. EDOT (0.05 M) monomers, Sodium dodecyl sulfate (0.2 M) and $LiClO_4$ (0.1 M) were dissolved in water for electrodeposition. Next, the sample was immersed in the solution and PEDOT was deposited on the interface between the hydrogel and conductive substrate by pluse electrodeposition (1.0 V vs Ag/AgCl, 1s, 0 V, 2s, 200 cycles). Finally, the interpenetrating ANF-PVA-PEDOT hydrogel electronics were peeled off from the electrodeposition mask.

Modeling and simulation.

In our discrete network simulations, 2D filamentous networks were generated by randomly placing 250 fiber, each with length l, into a box with dimension $2l \times 2l$ where periodic boundary conditions were enforced on each side of the box. A edge crack with length $0.5l$ was then introduced to the network (Fig. 2g). The fracture response of the network (when subjected to stretching in the vertical direction) was then simulated by treating each fiber as a Reissner beam[38] capable of undergoing large stretching and bending deformations. The mean distance of crosslinkes in the network is about 0.25 μm, which is consistent with experimental observation. The Young's modulus and diameter of fibre were chosen as E=18.2 GPa and d=50 nm, respectively, according to the tensile moduli of PVA and Kevlar 979 fiber (~960

Mpa and ~123 GPa).[39] Each pair of jointing fibres were assumed to be connected by a crosslinker modeled by a combined linear and rotational springs with spring constants of κ_s and κ_r respectively. Consequently, the strain energy stored in each deformed crosslinker is

$$E_c = \frac{1}{2}\kappa_s \delta l^2 + \frac{1}{2}\kappa_r \delta\theta^2$$

where δl is the separation of the intersecting points and $\delta\theta$ is the change in the relative angle between two filaments. In addition, once the energy reaches a critical value (i.e. the binding energy) E_m, the cross-linker will break and not rebind again. Adopted values of these parameters descrbing the response of crosslinkers are gathered in Table S1. Finally, possible re-alignment of fibres at the crack front was assessed by monitoring the the average value $\langle|\sin\theta|\rangle$ of all fibers within the circle (with diameter $0.2l$, see Figure S2) just in front of the crack tip where θ represents the angle formed between the filament and the horizontal axis.

A commercial software (ABAQUS) was used for FEA simulation of the designed kirigami membrane, treated as an elastic thin layer with prescribed cuts (Fig. 2i), at the continuum level. A small perturbation was applied perpendicular to the membrane to trigger the 3D out-of-plane deformation of kirigami structures. The minimum size of elements was set to be one third of the thickness of the kirigami membrane (~100μm). The elastic moduli (E) and Poisson's ratios (v) of various materials examined in this study are as follows: E_{CNFF}=45 MPa, v_{CNFF}=0.46; E_{Si}=165 GPa, v_{Si}=0.278; $E_{SU\text{-}8}$=2 GPa, $v_{SU\text{-}8}$=0.252.

Mechanical characterization

Tensile tester (Zwick Roel) was used to record the tensile response samples. Variations in the resistance of our specimens during uniaxial tensile and cyclic stretching tests were recorded by a digital source meter (2450; Keithley Instruments). Tearing tests was used to obtain the fracture toughness (Γ) of CNFF. Specifically, Γ was calculated according to the formular $\Gamma = 2F/t$, where F is the stable-state tearing force and t is the thickness of membrane.

Cell experiments

NIH 3T3 fibroblasts were used to examine the in vitro cytotoxicity of CNFF. The samples were washed with ethanol and phosphate buffered saline (PBS, Gibco™ pH 7.4 basic (1x)) prior to cell seeding. The cell suspension containing ~2×10^4 cells was seeded in culture plates containing the CNFF samples. The plates were placed in an incubator at 37℃ and 5% CO_2 after adding fresh medium, which was made by gentle mixing of 89% Dulbecco's modified eagle medium (DMEM, Gibco™, high glucose), 10% fetal bovine serum (Gibco™, qualified, Brazil), and 1% Penicillin-Streptomycin (Gibco™, 10,000 U/mL) in volume fraction. The live/dead assays were used to quantify the cell viability on day 1,3 and 5. Briefly, after discarding the culture medium, 200 µl PBS staining solution (Invitrogen™) including 2 µM calcein-AM and 8 µM propidium iodide (PI) was added into the plate and then cells were incubated at room temperature for 15 mins according to product instruction. Cells were observed using a fluorescent microscope (Nikon Eclipse Ci-L, Japan). Cell viability was defined by the normalized ratio of the number of living cells to the total number of cells, where the live/dead status of around 600-700 cells on at least 3 hydrogel samples was collected for each day's vitability.

Physiological recordings.

The array of multifunctional sensors includes four unipolar electrodes, one pair of bipolar electrodes and one temperature sensor. On the other hand, the design for conducting polymer structures involves six pairs of bipolar electrodes. Wafer-fabricated electrodes and conducting polymer electrodes attached to the chest of a volunteer can achieve high-quality ECG recording by a commercial data acquisition system (PowerLab T26, AD Instruments). Four wafer-fabricated unipolar electrodes attached to the forearm of a volunteer formed 2 independent channels to record EMG signals for gesture recognition. Skin impedance and temperature were recorded with a LCR meter (E4980AL; Keysight Instruments). All human

experiments were performed upon approval from the Human Research Ethics Committee, The University of Hong Kong under project number EA1812001. In addition, written consent was acquired from the participants of the research.

Supporting Information

Supporting Information is available from the Wiley Online Library or from the author.

Acknowledgements:

These authors contributed equally: Hongzhen Liu, Hegeng Li and Zuochen Wang. Author contributions: L.X. conceived the idea and supervised the research. Hongzhen Liu developed methods for fabricating CNFF membranes and infiltrated conducting polymers and carried out characterization of CNFF membranes. Hegeng Li developed processing techniques for wafer-fabricated devices and their integration onto CNFF membranes. Hegeng Li also carried out FEA simulation and physiological measurements, and prepared data figures for the manuscript. Z.W. contributed to the patterning of conductive composites, characterization of CNFF, and transfer printing of wafer-fabricated devices. X.W. and Y.L. carried out simulation of fibrillar network. H.Z. carried out cell experiments. M.S. assisted on the development of fabrication techniques. L.X. and Hegeng Li co-wrote the manuscript with assistance from the other authors. The study is supported by Research Grants Council (RGC), University Grants Committee (UGC) (Project 27210019 and 17200320 to L.X.; 17210618 and 17210520 to Y.L.).

Conflict of Interest:

The authors declare no conflict of interest.

Received: ((will be filled in by the editorial staff))
Revised: ((will be filled in by the editorial staff))
Published online: ((will be filled in by the editorial staff))

References

[1] Z. Huang, Y. Hao, Y. Li, H. Hu, C. Wang, A. Nomoto, T. Pan, Y. Gu, Y. Chen, T. Zhang, W. Li, Y. Lei, N. H. Kim, C. Wang, L. Zhang, J. W. Ward, A. Maralani, X. Li, M. F. Durstock, A. Pisano, Y. Lin, S. Xu, *Nat. Electron.* **2018**, *1*, 473.

[2] Y. Dai, H. Hu, M. Wang, J. Xu, S. Wang, *Nat. Electron.* **2021**, *4*, 17.

[3] N. Matsuhisa, X. Chen, Z. Bao, T. Someya, *Chem. Soc. Rev.* **2019**, *48*, 2946.

[4] D. C. Kim, H. J. Shim, W. Lee, J. H. Koo, D. H. Kim, *Adv. Mater.* **2020**, *32*, 1902743.

[5] Y. Wang, C. Zhu, R. Pfattner, H. Yan, L. Jin, S. Chen, F. Molina-Lopez, F. Lissel, J. Liu, N. I. Rabiah, Z. Chen, J. W. Chung, C. Linder, M. F. Toney, B. Murmann, Z. Bao, *Sci. Adv.* **2017**, *3*, e1602076.

[6] S. Choi, S. I. Han, D. Jung, H. J. Hwang, C. Lim, S. Bae, O. K. Park, C. M. Tschabrunn, M. Lee, S. Y. Bae, J. W. Yu, J. H. Ryu, S. W. Lee, K. Park, P. M. Kang, W. B. Lee, R. Nezafat, T. Hyeon, D. H. Kim, *Nat. Nanotechnol.* **2018**, *13*, 1048.

[7] C. Wang, C. Wang, Z. Huang, S. Xu, *Adv. Mater.* **2018**, *30*, 1801368.

[8] J. A. Fan, W.-H. Yeo, Y. Su, Y. Hattori, W. Lee, S.-Y. Jung, Y. Zhang, Z. Liu, H. Cheng, L. Falgout, M. Bajema, T. Coleman, D. Gregoire, R. J. Larsen, Y. Huang, J. A. Rogers, *Nat. Commun.* **2014**, *5*, 3266.

[9] Y. Wang, L. Yin, Y. Bai, S. Liu, L. Wang, Y. Zhou, C. Hou, Z. Yang, H. Wu, J. Ma, Y. Shen, P. Deng, S. Zhang, T. Duan, Z. Li, J. Ren, L. Xiao, Z. Yin, N. Lu, Y. A. Huang, *Sci. Adv.* **2020**, *6*, eabd0996.

[10] L. Xu, S. R. Gutbrod, A. P. Bonifas, Y. Su, M. S. Sulkin, N. Lu, H.-J. Chung, K.-I. Jang, Z. Liu, M. Ying, C. Lu, R. C. Webb, J.-S. Kim, J. I. Laughner, H. Cheng, Y. Liu, A. Ameen, J.-W. Jeong, G.-T. Kim, Y. Huang, I. R. Efimov, J. A. Rogers, *Nat. Commun.* **2014**, *5*, 3329.

[11] S. Han, M. K. Kim, B. Wang, D. S. Wie, S. Wang, C. H. Lee, *Adv. Mater.* **2016**, *28*, 10257.

[12] Y. Xu, B. Sun, Y. Ling, Q. Fei, Z. Chen, X. Li, P. Guo, N. Jeon, S. Goswami, Y. Liao, S. Ding, Q. Yu, J. Lin, G. Huang, Z. Yan, *Proc. Natl. Acad. Sci. U. S. A.* **2020**, *117*, 205.

[13] L. Tian, B. Zimmerman, A. Akhtar, K. J. Yu, M. Moore, J. Wu, R. J. Larsen, J. W. Lee, J. Li, Y. Liu, B. Metzger, S. Qu, X. Guo, K. E. Mathewson, J. A. Fan, J. Cornman, M. Fatina, Z. Xie, Y. Ma, J. Zhang, Y. Zhang, F. Dolcos, M. Fabiani, G. Gratton, T. Bretl, L. J. Hargrove, P. V. Braun, Y. Huang, J. A. Rogers, *Nat. Biomed. Eng.* **2019**, *3*, 194.

[14] Z. Li, M. Zhu, J. Shen, Q. Qiu, J. Yu, B. Ding, *Adv. Funct. Mater.* **2019**, *30*, 1908411.

[15] Y. Zhang, T. Zhang, Z. Huang, J. Yang, *Adv. Sci.* **2022**, 2105084.

[16] D.-H. Kim, J. Viventi, J. J. Amsden, J. Xiao, L. Vigeland, Y.-S. Kim, J. A. Blanco, B. Panilaitis, E. S. Frechette, D. Contreras, D. L. Kaplan, F. G. Omenetto, Y. Huang, K.-C. Hwang, M. R. Zakin, B. Litt, J. A. Rogers, *Nat. Mater.* **2010**, *9*, 511.

[17] S. Liu, Y. Rao, H. Jang, P. Tan, N. Lu, *Matter* **2022**, *5*, 1104.

[18] M. K. Blees, A. W. Barnard, P. A. Rose, S. P. Roberts, K. L. McGill, P. Y. Huang, A. R. Ruyack, J. W. Kevek, B. Kobrin, D. A. Muller, P. L. McEuen, *Nature* **2015**, *524*, 204.

[19] T. C. Shyu, P. F. Damasceno, P. M. Dodd, A. Lamoureux, L. Xu, M. Shlian, M. Shtein, S. C. Glotzer, N. A. Kotov, *Nat. Mater.* **2015**, *14*, 785.

[20] Y. Morikawa, S. Yamagiwa, H. Sawahata, R. Numano, K. Koida, M. Ishida, T. Kawano, *Adv. Healthc. Mater.* **2018**, *7*, 1701100.

[21] A. Lamoureux, K. Lee, M. Shlian, S. R. Forrest, M. Shtein, *Nat. Commun.* **2015**, *6*, 7373.

[22] K. Yong, S. De, E. Y. Hsieh, J. Leem, N. R. Aluru, *Mater. Today* **2020**, *34*, 58.

[23] L. Xu, T. C. Shyu, N. A. Kotov, *ACS Nano* **2017**, *11*, 7587.

[24] H. Li, H. Liu, M. Sun, Y. Huang, L. Xu, *Adv. Mater.* **2020**, *33*, 2004425.

[25] R. Zhao, S. Lin, H. Yuk, X. Zhao, *Soft Matter* **2018**, *14*, 2515.

[26] J. Zhu, M. Yang, A. Emre, J. H. Bahng, L. Xu, J. Yeom, B. Yeom, Y. Kim, K. Johnson, P. Green, *Angew. Chemie Int. Ed.* **2017**, *56*, 11744.

[27] L. Xu, X. Zhao, C. Xu, N. A. Kotov, *Adv. Mater.* **2018**, *30*, 1703343.

[28] R. C. Picu, *Soft Matter* **2011**, *7*, 6768.

[29] S. Zhao, W. J. Malfait, N. Guerrero-Alburquerque, M. M. Koebel, G. Nyström, *Angew. Chemie Int. Ed.* **2018**, *57*, 7580.

[30] J.-Y. Sun, X. Zhao, W. R. K. Illeperuma, O. Chaudhuri, K. H. Oh, D. J. Mooney, J. J. Vlassak, Z. Suo, *Nature* **2012**, *489*, 133.

[31] A. Das, A. Sinha, V. R. Rao, K. N. Jonnalagadda, *Exp. Mech.* **2017**, *57*, 687.

[32] C. P. Broedersz, X. Mao, T. C. Lubensky, F. C. MacKintosh, *Nat. Phys.* **2011**, *7*, 983.

[33] X. Wei, Q. Zhu, J. Qian, Y. Lin, V. B. Shenoy, *Soft Matter* **2016**, *12*, 2537.

[34] R. Ballarini, R. L. Mullen, Y. Yin, H. Kahn, S. Stemmer, A. H. Heuer, *J. Mater. Res.* **1997**, *12*, 915.

[35] M. Pharr, Z. Suo, J. J. Vlassak, *Nano Lett.* **2013**, *13*, 5570.

[36] J. Lyu, X. Wang, L. Liu, Y. Kim, E. K. Tanyi, H. Chi, W. Feng, L. Xu, T. Li, M. A. Noginov, C. Uher, M. D. Hammig, N. A. Kotov, *Adv. Funct. Mater.* **2016**, *26*, 8435.

[37] H. Li, Z. Wang, M. Sun, H. Zhu, H. Liu, C. Y. Tang, L. Xu, *Adv. Funct. Mater.* **2022**, 2202792. DOI:10.1002/adfm.202202792

[38] Crisfield, M. A. Non-linear finite element analysis of solids and structures. Ch7, John Wiley & Sons, NewYork, 1997.

[39] X. Zheng, H. Lee, T. H. Weisgraber, M. Shusteff, J. DeOtte, E. B. Duoss, J. D. Kuntz, M. M. Biener, Q. Ge, J. A. Jackson, *Science.* **2014**, *344*, 1373.

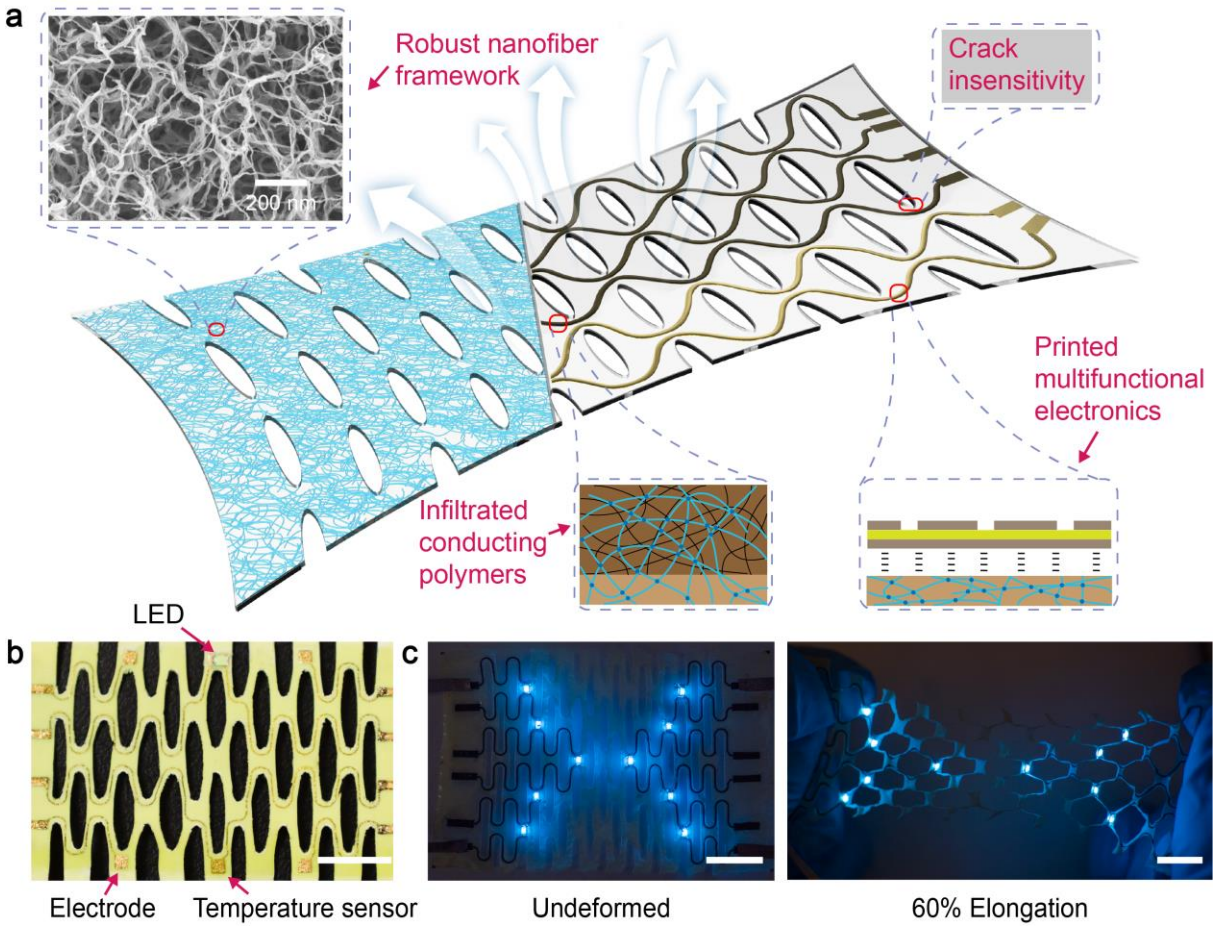

Figure 1. Robust and multifunctional kirigami electronics based on CNFF. (**a**) Schematic of a CNFF-based kirigami membrane with transfer-printed microelectronics and infiltrated conducting polymers. (**b**) Actual image showing a CNFF-based kirigami membrane with integrated multifunctional electronics including LED, bioelectrodes and temperature sensor. Scale bar: 10 mm. (**c**) Photographs of CNFF-based kirigami electronics showing a stretchable LED array powered with serpentine interconnects from conducting polymers. Scale bar: 10 mm.

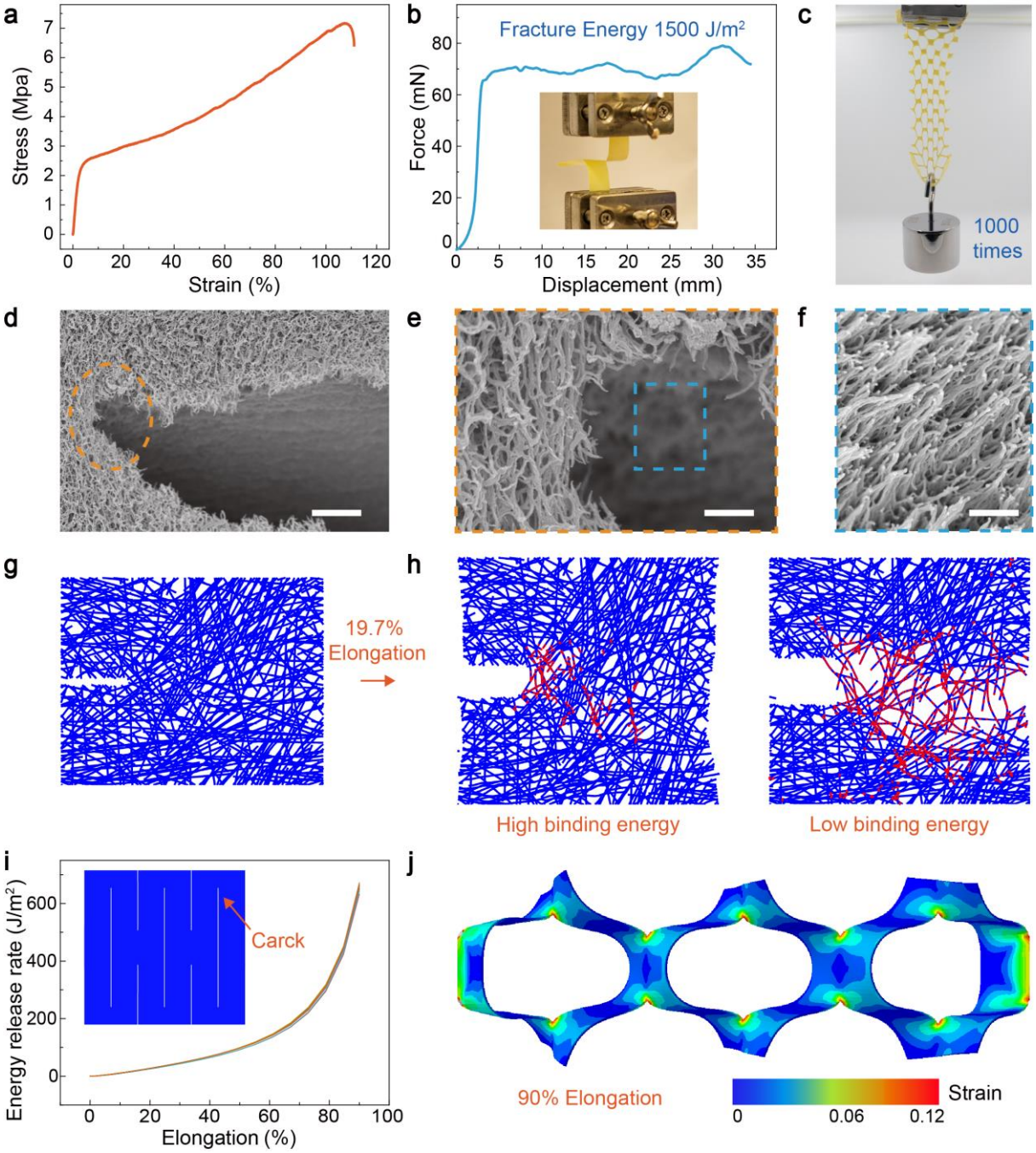

Figure 2. Fracture resistance of CNFF-based kirigami membranes. (**a**) Recorded tensile response of a continuous CNFF membrane. (**b**) Fracture energy of CNFF determined by standard tearing test. (**c**) A CNFF-based kirigami membrane capable of bearing a weight of 250g, demonstrating its high mechanical strength. (**d-f**) Scanning electron microscope (SEM) images of the fracture surface of CNFF, showing microstructural basis of its high toughness. Scale bar: 5 μm (**d**), 1 μm (**e**), 500 nm (**f**). (**g**) Computational model of a crosslinked fibrillar network with an initial crack. (**h**) Distinct levels of fibrillar binding energy (equal to E_m or 0.4 E_m, with the value of E_m given in Table S1) led to different responses of the crack-incorporated fibrillar network under imposed elongation. Red dots represent sites where crosslinking breakage takes place. (**i**) Energy release rate for crack propagation, as a function of the elongation imposed on a CNFF-based kirigami membrane, revealed by finite element analysis (FEA). The inset shows the geometry of the kirigami pattern. (**j**) Strain distribution in the CNFF-based kirigami membrane, undergoing to 100% elongation, from the FEA simulation.

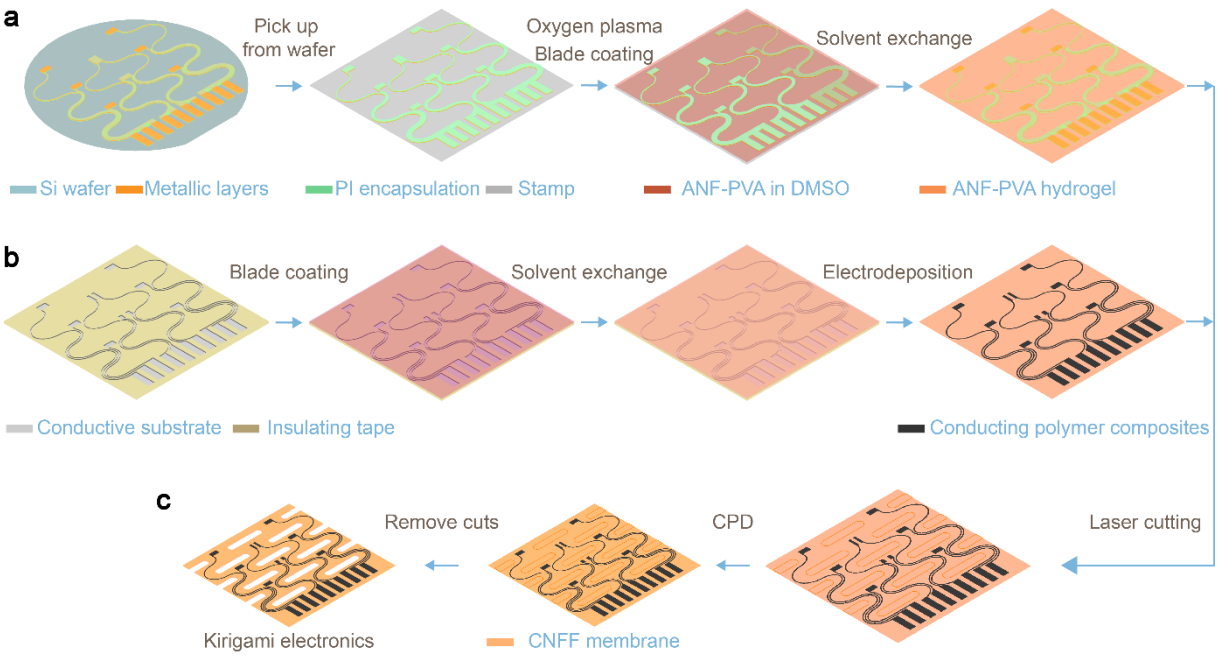

Figure 3. Schematics of the fabrication processes for CNFF-based kirigami electronics. (**a**) Transferring methods for wafer-fabricated multifunctional electronics. (**b**) Electrodeposition processes for the integration of conducting polymers. (**c**) Laser cutting and CPD steps complete the fabrication of CNFF-based kirigami electronics.

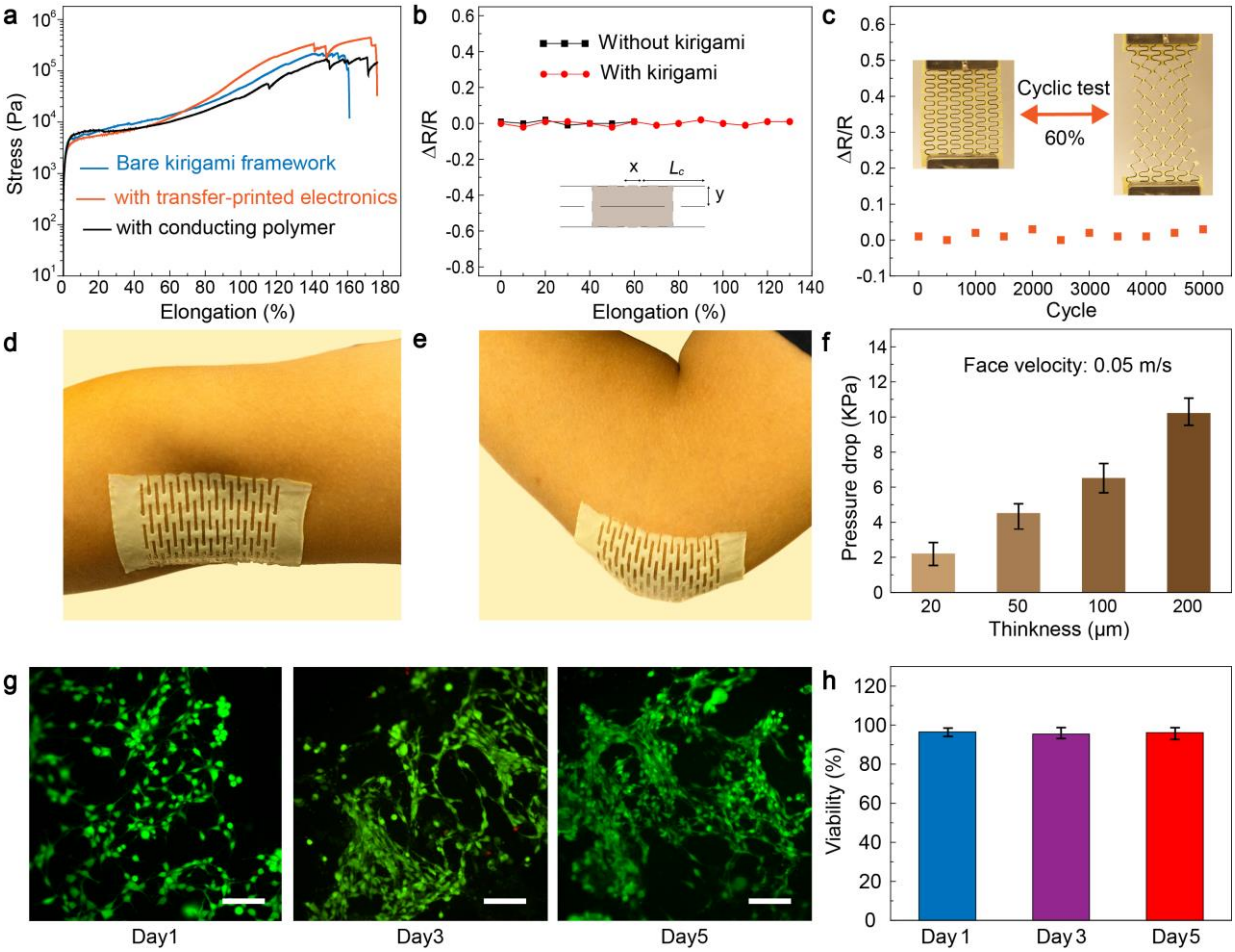

Figure 4. Behaviors of CNFF-based kirigami devices for wearable applications. (**a**) Tensile responses of a bare kirigami membrane and kirigami membranes with transfer-printed serpentine electronics or infiltrated conducting polymer interconnects. (**b**) Resistance variation for conducting polymer interconnects as a function of elongation imposed to CNFF membranes with or without kirigami cuts. (**c**) Resistance variation of conducting polymer interconnects under 5,000 cycles of 60% elongation imposed to the kirigami membrane. (**d-e**) A CNFF-based kirigami membrane conforming to the 3D dynamic surface of human skin. (**f**) Air flow though CNFF membranes with various thickness led to moderate pressure drop across the membrane, demonstrating good permeability of the CNFF. (**g**) Live/dead assay of NIH 3T3 fibroblasts cultured on CNFF membrane for 1, 3 and 5 days. Live cells: green. Dead cells: red. Scale bars: 100 μm (**h**) Cell viability over 5 days of incubation.

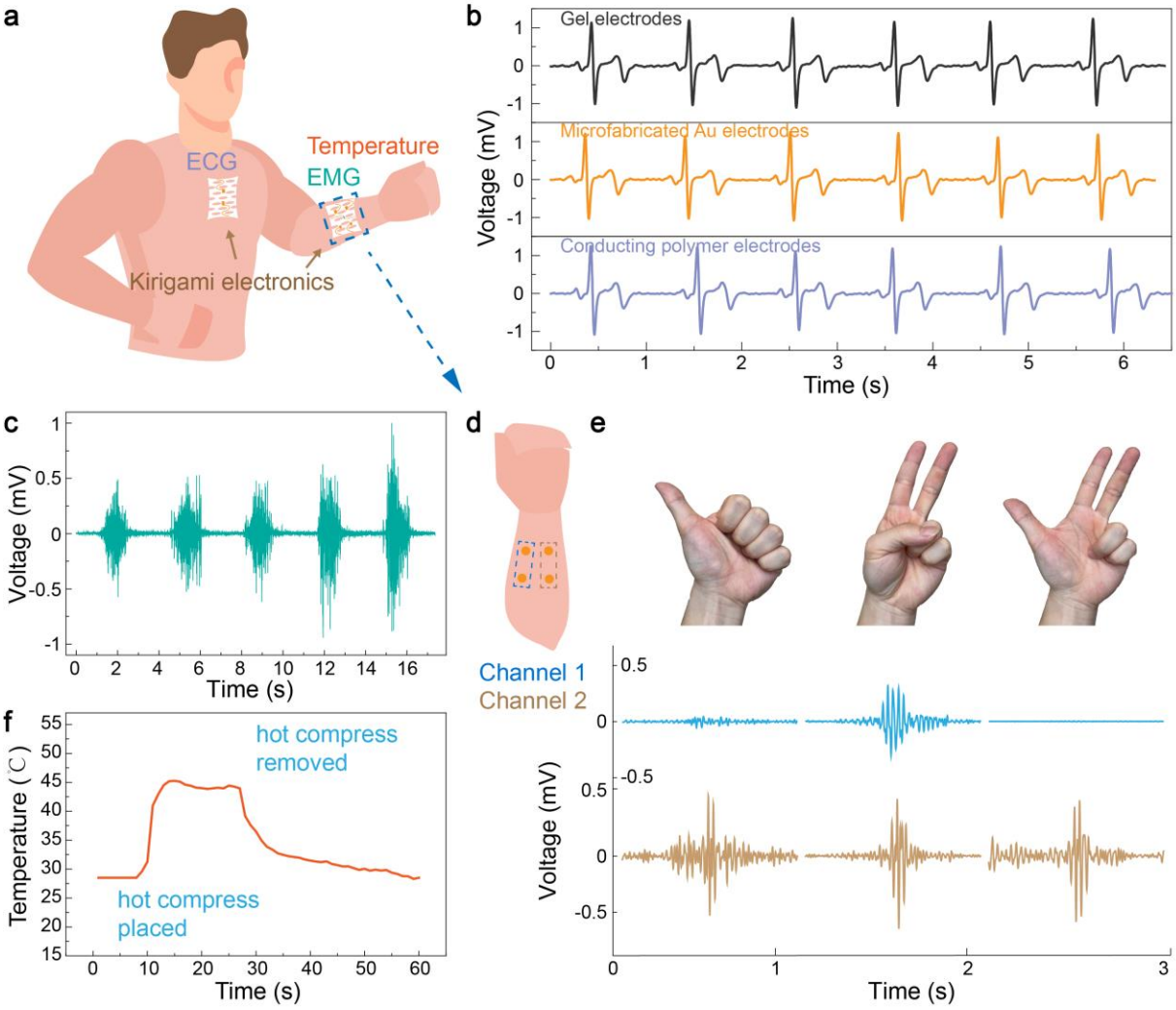

Figure 5. Multimodal physiological sensing with CNFF-based kirigami electronics. (**a**) Schematic showing the capability of multifunctional kirigami devices for sensing various biological signals. (**b**) ECG data measured with microfabricated Au electrodes (middle) and conductive polymer electrodes (bottom) integrated on CNFF-based kirigami membranes, as compared with the data measured with commercial gel electrodes (top). (**c**) An EMG recording with CNFF-based kirigami electronics. (**d-e**) Two pairs of microfabricated Au electrodes laminated on the forearm (**d**) form two independent channels for EMG-based gesture recognition (**e**). (**f**) Temperature variation during a hot compress applied to the skin, recorded by a microfabricated sensor integrated on the kirigami membrane.